

Photophysical properties of Eu^{3+} complexes approaching electronic contact to a metal surface

Adrian Ebert,[†] Simon Fromme,[†] Lisa Burgert,[†] Umar Rashid,[†] Lukas Gerhard,^{*,†} Julia Feye,[‡] Senthil Kumar Kuppusamy,[†] Barbora Brachnakova,[†] Timo Neumann,[¶] Mario Ruben,^{§,†,||} Peter W. Roesky,[‡] Michael Seitz,[¶] and Wulf Wulfhekel[†]

[†]*Institute for Quantum Materials and Technologies, Karlsruhe Institute of Technology (KIT),
D-76344 Eggenstein-Leopoldshafen, Germany*

[‡]*Institute for Inorganic Chemistry, Karlsruhe Institute of Technology, Karlsruhe, Germany*

[¶]*Institute of Inorganic Chemistry, University of Tübingen, Tübingen, Germany*

[§]*Institute of Nanotechnology, Karlsruhe Institute of Technology (KIT), D-76344
Eggenstein-Leopoldshafen, Germany*

^{||}*Centre Européen de Sciences Quantiques (CESQ), Institut de Science et d'Ingénierie
Supramoléculaires (ISIS), BP 70028, 67083, Strasbourg Cedex, France.*

E-mail: Lukas.Gerhard@kit.edu

Abstract

The application of rare-earth complexes in electrically driven light sources poses a series of challenges that require specific optimization of the molecular photophysical properties. Here, we present a report on films of three different Eu³⁺ complexes characterized in terms of emission spectra and fluorescence decay. We compare molecular complexes in powder form and sublimed films, in films on glass and on a metal surface, and in films of thicknesses down to less than 3 nm (< 3 ML), approaching electrical coupling. Our photoluminescence experiments supported by scanning tunneling microscopy of sub-monolayers indicate that Eu³⁺ trisal-complexes are less affected by sublimation and more stable on the metal surface than typical beta diketonate complexes, making them promising candidates for electroluminescence devices.

Introduction

Miniaturization of electronic devices with the ultimate goal of electrically controlled single-molecule devices by exploiting intrinsic quantum properties requires a comprehensive understanding of the wide range of effects that occur in the presence of a metal. Rare-earth complexes appear to be ideally suited for nanoscale opto-electronic devices, based on their high ligand-based absorption and strong rare-earth ion luminescence, sharp and environment-insensitive emission spectra, and rich photophysics.^{1,2} Functional electronic devices intrinsically require electrodes to make electrical contact with the organic moiety. For light in the visible range, typical electrode metals such as Ag act as a mirror changing the photonic mode density of a nearby emitter, which has been the subject of research since the pioneering experiments of Drexhage.³⁻⁹ Depending on the structure and nature of the metal electrode, coupling of molecular excitons to plasmons leads to quenching^{7,10-12} or enhancement of the light emitted in the far field.¹³⁻¹⁷ Electroluminescence,¹⁸ which refers to the luminescence of electrically excited molecules, intrinsically requires some degree of electrical contact to an electrode, which leads to additional potential de-excitation by tunneling of charge carriers at very small distances to the electrodes. Fluorescence of films com-

posed of organic chromophores has been explored at small distances from metal surfaces in the past^{19,20} and no indication for the onset of exciton quenching via tunneling has been found for distances down to about 1 nm. However, it is not straightforward to transfer these results to radiating 4f excitations of lanthanide (Ln) ions: On the one hand, the vastly different radiative lifetimes ($\approx 10^{-9}$ s in typical chromophores vs $\approx 10^{-3}$ s in Ln ions) suggest that drastically enhanced decoupling from the metal surface would be required. On the other hand, the localized nature of the 4f excitations already significantly isolates the excitations from the environment. In addition, the small cross-section of 4f excitations typically makes excitation via antenna ligands and an efficient intra-molecular energy transfer to the Ln ion necessary. Besides these direct optical and electrical effects on the light emission, a metal surface also affects growth of adsorbed molecular complexes and even facilitates fragmentation.²¹ Finally, rare-earth complexes are prone to bleaching under repeated optical excitation, an effect that has recently been linked to reduction²² and that might be affected by the electron bath of a nearby metal as well.

This calls for a systematic study of the optical properties of Ln complexes in very close proximity to a metal surface under well-controlled conditions.

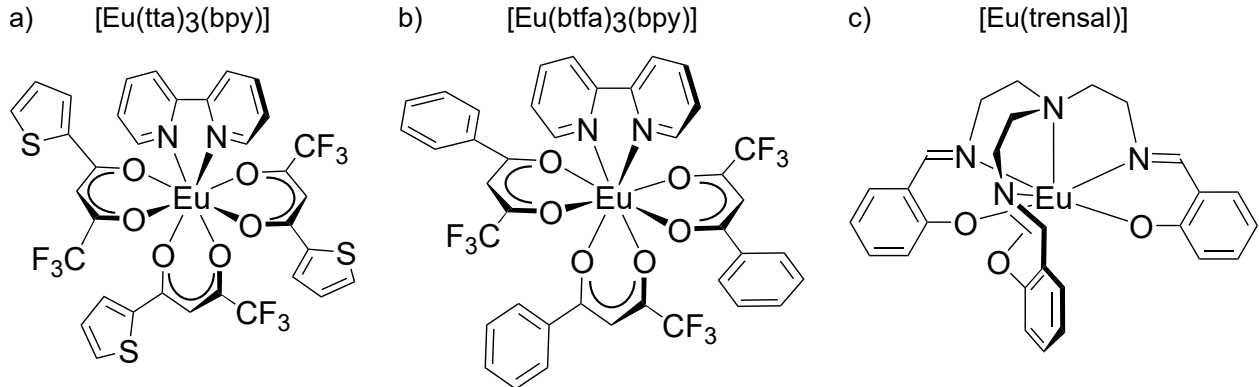


Figure 1: Structure representation of $[\text{Eu}(\text{tta})_3(\text{bpy})]$, $[\text{Eu}(\text{btfa})_3(\text{bpy})]$ and $[\text{Eu}(\text{trensal})]$ complexes.

Here, we report on characterization of the thin film growth of $[\text{Eu}(\text{tta})_3(\text{bpy})]$ ^{23–27} (Fig. 1 (a)), $[\text{Eu}(\text{btfa})_3(\text{bpy})]$ ^{25,27–30} (Fig. 1 (b)) and $[\text{Eu}(\text{trensal})]$ ³¹ (Fig. 1 (c)) complexes on glass and Ag substrates under ultra-high vacuum conditions. Photoluminescence spectra (PL) and time-correlated single photon counting (TCSPC) of thin films down to about 3 monolayers (ML) show evidence

of strong PL quenching of luminescence due to electromagnetic coupling to the flat metal surface and significant bleaching in the absence of oxygen at 4.5 K. Both PL and scanning tunneling microscopy (STM) of sub-monolayers indicate that [Eu(trensal)] is less affected by sublimation than the two beta diketonate complexes.³²

Experimental

Optical set-up

Low-temperature STM measurements were performed using a custom-built ultra-high vacuum (UHV) STM operating at 4.5 K and a base pressure of approximately 10^{-10} mbar.³³

PL spectra were acquired using a spectrometer with a focal length of 150 mm and a diffraction grating of 300 grooves/mm. The maximum spectral resolution of the system is approximately 2 nm with a slit width of 10 μ m, but for most spectra presented here spectral resolution has been traded for detection efficiency. All photon spectra presented are corrected for the wavelength-dependent collection efficiency of the detection setup. Excited-state lifetimes were determined via TCSPC using a single photon avalanche diode (SPAD) for detection with bandpass filter of 610 ± 10 nm. Two set-ups were used for PL measurements, both with sample and optical fibers in UHV conditions. Set-up a) (Fig. 2 (a)) features two multimode fibers (diameter 200 μ m) positioned at an angle about half a mm away from the sample. One optical fiber guides the light for excitation towards the sample at room temperature (RT), the other one collects the PL response and guides it towards the SPAD for TCSPC measurements, or towards the spectrometer. The plane defined by the two optical fibers is tilted with respect to the sample to minimize collection of reflected light. Set-up b) (Fig. 2 (b)) features only one multimode fiber (diameter 200 μ m) positioned perpendicular to the sample at a distance of about 30 μ m inside the cryostat at a temperature of 4.5 K.

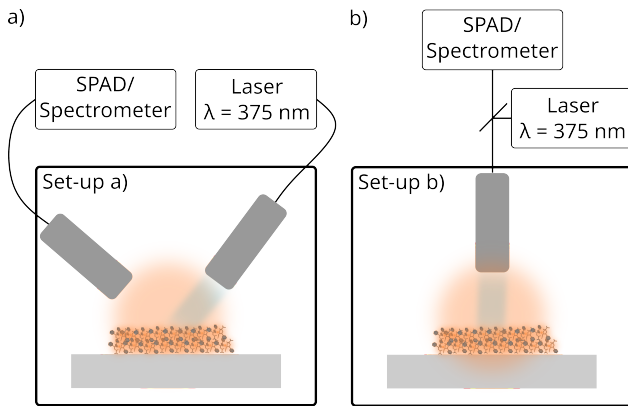


Figure 2: Schematic drawings of the photoluminescence (PL) set-ups. a) Two optical fibers positioned at an angle and about 0.5 mm from the sample for excitation and collection of the PL response. b) Single optical fiber positioned perpendicular to the sample at a distance of about 30 μm .

Sample preparation

The complexes were synthesized according to.^{28,34} Ag(111) single-crystal substrate was prepared by repeated cycles of argon ion sputtering (1.5 keV), followed by annealing at temperatures between 500 and 600 $^{\circ}\text{C}$. Thermal sublimation of $[\text{Eu(btfa)}_3(\text{bpy})]$, $[\text{Eu(tta)}_3(\text{bpy})]$, and $[\text{Eu(trensal)}]$ complexes was carried out using a Kentax three-cell evaporator. The areal densities of the sublimed films were calibrated using a quartz microbalance and their thickness was estimated using the volume densities from the literature.³⁵ Molar mass allows to estimate The thicknesses in molecules per nm^2 can be calculated by dividing the areal density by the molar mass.

Results and discussion

Comparison of photophysical properties of powder and thin films of $[\text{Eu(btfa)}_3(\text{bpy})]$, $[\text{Eu(tta)}_3(\text{bpy})]$ and $[\text{Eu(trensal)}]$

$[\text{Eu(btfa)}_3(\text{bpy})]$, $[\text{Eu(tta)}_3(\text{bpy})]$ and $[\text{Eu(trensal)}]$ complexes were sublimed with a thickness of ~ 22.5 molecules/ nm^2 ($\approx 21 \text{ nm}$ in case of $[\text{Eu(tta)}_3(\text{bpy})]$) on glass (microscope slide) and Ag(111) substrates in UHV. Excitation with $\lambda = 375 \text{ nm}$ results in the emission spectra shown in the left

panels of Fig. 3 with the well known series of emission bands corresponding to transitions from the excited 5D_0 to the $7F_{J=0-4}$ ground states of the Eu³⁺ ion.³⁶ All PL spectra were normalized to the magnetic transition $D_0 \rightarrow F_1$. The right panels display the corresponding time evolution of the PL intensity of the main peak corresponding to the $^5D_0 \rightarrow ^7F_2$ transition. This peak is dominant for all samples, giving the Eu³⁺ emission its characteristic red color.

To discuss the variations of the emitted light, we note that four different mechanisms affect the PL spectra and fluorescence lifetimes. First, there can be chemical changes³⁷ or differences in the molecular arrangement in the three types of samples affecting the emission spectra. Second, the emission characteristics are affected by the optical environment of the molecules. In powder, it is isotropic, the vacuum-glass interface provides a discontinuity in the refractive index, and the metallic Ag substrate is reflective.^{4,38} Third, on the metallic substrate surface plasmons may interact with the molecules.¹¹ Finally, emission can be quenched by electronic hybridization of 4f states and the conduction electrons of the metal substrate.

The highest energy $^5D_0 \rightarrow ^7F_0$ transition is strictly forbidden according to the standard Judd-Ofelt theory but can be induced by J mixing caused by the ligand field.^{36,39-43} This emission band can easily be seen in the sublimed samples of [Eu(btfa)₃(bpy)] and [Eu(tta)₃(bpy)] on both substrates while it is nearly absent in the powder sample. This indicates a modified ligand field effect in the sublimed samples, which might be explained by a deformation due to a different intermolecular arrangement in the film or even the cleavage of one of the ligands by sublimation.³²

This is supported by the observation that the individual stark levels of the $^5D_0 \rightarrow ^7F_2$ and the $^5D_0 \rightarrow ^7F_4$ bands are sharper in the emission of [Eu(btfa)₃(bpy)] and [Eu(tta)₃(bpy)] in powder compared to the sublimed films, while they are similar for the [Eu(trensal)] samples (see left panels of Fig. 3).

To qualitatively compare the dynamics of the light emitting excited states of the three different complexes, we measured the decay of the intensity of the $^5D_0 \rightarrow ^7F_2$ transition (bandpass filter of 610 ± 10 nm) after prolonged illumination (0.1 to 0.5 ms, $\lambda = 375$ nm) as shown in Figure 3 (d)-(f). The experimental data deviates from a single exponential decay in particular in the sublimed

films, which is why a fit with a sum of two exponential decays is shown. This deviation indicates that Eu ions experience different local environments, possibly depending on the distances to the underlying substrate.

Comparing the overall emission dynamics of the three complexes, [Eu(trensal)] shows about a factor of two shorter lifetimes in powder form ($\approx 800 \mu\text{s}$ vs $\approx 400 \mu\text{s}$) and also mostly in the films (see Fig. 3 (d)-(f)), in agreement with previous work.^{27,31,44} For [Eu(tta)₃(bpy)] and [Eu(btfa)₃(bpy)], the observed lifetime τ_{obs} in thin sublimed films is clearly shorter than in powder, in agreement with our previous work and early literature^{27,38} (see Fig. 3 (d),(e)), while this effect is less pronounced for [Eu(trensal)]. Together with the changes in the PL spectra, this indicates that sublimation of [Eu(btfa)₃(bpy)] and [Eu(tta)₃(bpy)] which have C1 symmetry, has more pronounced consequences in terms of lack of crystallinity and integrity of the complexes. The [Eu(trensal)] ligand structure with C3 symmetry seems to be more robust compared to beta diketonates [Eu(tta)₃(bpy)] and [Eu(btfa)₃(bpy)].

In addition to reduced symmetry in the sublimed films, hydroxyl groups on the glass surface can lead to quenching of nearby emitters via phonons.

In addition to the increased structural disorder in the sublimed film, increased refractive index of the surrounding medium³⁶ (glass vs. air) and the discontinuous jump in the refractive index modifying the photonic density of states at the interface may be reasons for increased radiative decay for films on glass. The controlled growth of thin films on glass is beyond the scope of this paper and we therefore refrain from quantitative analysis of the observed decay rates (estimation of radiative rates based on Judd-Ofelt analysis).

The magnetic dipole transition $^5D_0 \rightarrow ^7F_1$ is typically assumed to be less sensitive to the local environment, and thus the corresponding radiative decay rate is approximately constant for all Eu³⁺ complexes.³⁶ Based on this assumption, the relative intensities of the other transitions are proportional to the corresponding radiative decay rates.^{36,45}

Note that on the metal surface, the modes of the electromagnetic field with a wave vector normal to the surface display a node in the electric field and a maximum in the magnetic field near

the interface due to boundary conditions. As our setup (see Fig. 2) mainly detects light emitted normal to the surface, this property leads to a relative suppression of the electric dipole emission normal to the surface compared to that of the magnetic dipole emission. When the spectra are normalized to the magnetic transition intensity, this effect manifests as a relative decrease of the measured electric dipole peaks as observed in all spectra on Ag(111).

The Ag surface leads to dissipation of molecular excitations in its vicinity via plasmon excitation depending on the orientation of the transition dipole moment with respect to the substrate, the distance to the substrate and the geometry of the substrate,^{4,11,46–50} which leads to a rather large variation within nominally identical films. A more detailed study of the influence of [Eu(tta)₃(bpy)] film thickness on the fluorescence decay is discussed below.

Hybridization of the 4f states of Eu³⁺ and the metal substrate that allows charge transport with time constants comparable to the PL lifetime would drastically suppress photon emission, which we have not observed, despite a significant conductance across molecular layers as shown by the STM topography in Figure 3 f).

Photophysical properties of [Eu(tta)₃(bpy)] as a function of its film thickness

To quantitatively investigate the impact of the metal substrate on light emission, films of [Eu(tta)₃(bpy)] with densities between 3 and 15 molecules · nm⁻² were sublimed on a flat Ag(111) single crystal. Here we were careful to keep the exact same conditions for the film growth for different thicknesses in order to allow a direct comparison. Assuming a density of 1.7 g · cm⁻³³⁵ the areal density calibrated by the quartz balance translates to thicknesses of 2.8 to 14.1 nm. PL spectra and TCSPC were measured at 4.5 K with an optical fiber placed \approx 30 μ m above the film (see Fig. 2 (b)). As discussed above, the different boundary conditions of the electric and magnetic components of the electromagnetic field at the metal surface in combination with our detection setup perpendicular to the surface favor MD emission over ED emission. This effect is strongly enhanced for thinner films. For the thinnest film, the MD $^5D_0 \rightarrow ^7F_1$ transition is even more intense than the ED $^5D_0 \rightarrow ^7F_2$ transition (see Fig. 4(a)). In addition, the overall integrated inten-

sity per molecule of the emission spectra drastically decreases with decreasing film thickness. The TCSPC measurements, performed for each film thickness, show that the decay rates drastically increase with decreasing film thickness (see Fig. 5). If approximated by a single exponential decay, the observed decay rate scales as $\gamma_{\text{obs}} \propto d^{-2.9}$ (see Fig. 4 (b)).

This is well expected for radiation being dissipated into the nearby metal in form of plasmons. At short distances, the dissipation rate γ_{quench} of dipolar emission in the metal bulk is proportional to the radiative rate in free space γ_{rad0} and the distance d to the power 3 between the molecular emitter and the metal surface.^{12,51-53}

$$\begin{aligned}\gamma_{\text{quench}} &= \gamma_{\text{rad0}} \cdot \frac{3}{16k^3} \text{Im} \left(\frac{\varepsilon(\omega) - \varepsilon(\text{mol})}{\varepsilon(\omega) + \varepsilon(\text{mol})} \right) \cdot \frac{p_x^2 + p_y^2 + 2p_z^2}{|\mathbf{p}|^2} \cdot \frac{1}{d^3} \\ &\approx \gamma_{\text{rad0}} \cdot \frac{4030}{(d[\text{nm}])^3}\end{aligned}\quad (1)$$

Here, we approximated $\lambda = 615$ nm (corresponding to the $^5D_0 \rightarrow ^7F_2$ transition), $\varepsilon(\text{mol})=2.56^{36}$ and $\varepsilon(\omega) = -16+0.6i^{54}$ denote the permittivities of the metal surface and the molecular film, respectively. A random orientation of the transition dipoles results in $\frac{p_x^2 + p_y^2 + 2p_z^2}{|\mathbf{p}|^2} = 4/3$. In this way, the decay can be estimated from literature values as $\gamma_{\text{obs}} = \gamma_{\text{rad0}} * (1 + \frac{4030}{(d[\text{nm}])^3}) + \gamma_{\text{nonrad}}$. Note that the energy transferred to the substrate in the form of plasmonic excitations is unlikely to be radiated to the far field for the present case, because of the momentum mismatch between the plasmomic modes of the atomically flat Ag(111) that we chose for simplicity and the radiative modes in the far field. As the film growth mode is unknown, we compare our experimental data to two scenarios: a perfect 2D growth with vanishing roughness of the film and a Poisson distribution of molecules (3D growth). In this way, we can model the decay of each film as a superposition of individual layers with the corresponding distance dependent decay rate. This leaves only a global factor as a free parameter that includes excitation/detection efficiency and which amounts to a constant offset in the logarithmic plots. As is shown in Figure 5, the experimental data indeed falls right in between the extreme scenarios of 2D and 3D growth for all thicknesses. This indicates no significant additional quenching pathways e.g. via electron transport.

If the molecular decay constants are known in bulk, equation 1 can be used to estimate the distance of a emitter from the surface from its PL decay. In a film, the distribution of the distances of the emitters from the surface can be estimated by fitting a sum of exponentials with decay constants corresponding to equally spaced distances to the experimental decay. Here, we use $d = 0, 2, 4, \dots, 20$ nm as a basis set (see Fig. 6). The resulting estimates for the distance distribution of the emitters agree well with the expected thickness distributions of the film with the nominal thickness determined by the quartz microbalance, in particular for the thicker films.

Decrease of fluorescence intensity under illumination

Bleaching by exposure to UV light is a well documented effect for Eu^{3+} complexes. Most studies focus on complexes in solution,⁵⁵ embedded in host matrices⁵⁶⁻⁵⁹ or single crystals⁶⁰ and are limited to qualitative conclusions. Since our ultimate aim is to investigate the luminescence of electrically contacted single molecules, we quantified the photo-degradation process of a $[\text{Eu}(\text{tta})_3(\text{bpy})]$ film with a density of around 22.5 molecules/nm² on Ag(111) under exposure to UV light with $\lambda = 375$ nm in UHV at $T = 4.5$ K. The PL spectrum was repeatedly recorded using the setup shown in Figure 2 (b). Figure 7 (a) shows that the intensity integrated over the whole spectral range and the intensity of the $^5D_0 - ^7F_2$ transition decrease significantly over time. The photo-bleaching lifetime of the $[\text{Eu}(\text{tta})_3(\text{bpy})]$ is estimated to be $\approx 6 \cdot 10^3$ s from an exponential fit to the time dependent intensity (see Fig. 7 (a)) and corresponds to an average number of about 10^5 photons emitted by each Eu complex before the initial intensity of the PL signal drops to 1/e. This photo-bleaching probability of the order of 10^{-5} is within the range of typical organic dyes in water and at room temperature ($10^{-3} - 10^{-7}$)⁶¹ but too high to perform extended single-molecule experiments. Within the margins of error due to limited wavelength resolution of the setup, there is no change of the emission energy (see Fig. 7b) and no appearance or disappearance of any peak (see Fig. 7 (c)) which would indicate fragmentation of the complex or reduction of Eu^{3+} to Eu^{2+} that has been previously reported.²²

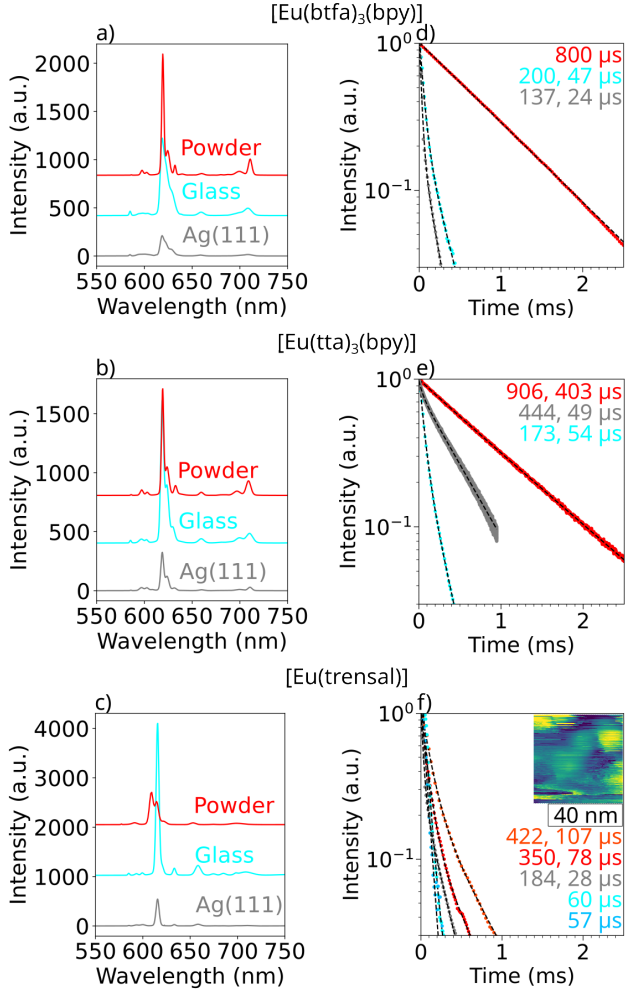
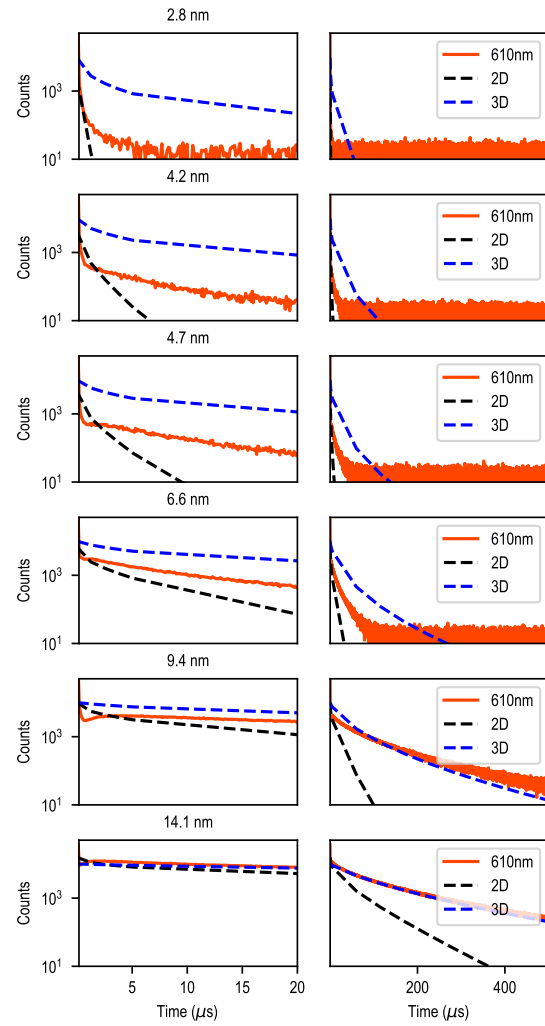
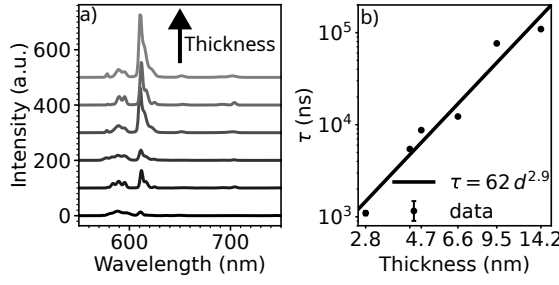


Figure 3: Photophysical properties of thin films of $[\text{Eu(btfa)}_3(\text{bpy})]$, $[\text{Eu(tta)}_3(\text{bpy})]$ and $[\text{Eu(trensal)}]$ under excitation with $\lambda = 375 \text{ nm}$. a)-c) PL spectra of powder and films sublimed onto glass and Ag(111) with a density of $\sim 22.5 \text{ molecules/nm}^2$ at RT. The intensity of the PL spectra has been normalized to the integrated intensity of the $^5D_0 \rightarrow ^7F_1$ transition. Graphs shifted for clarity. d)-f) Decay of the intensity of the $^5D_0 \rightarrow ^7F_2$ transition (recorded using a bandpass filter of $610 \pm 10 \text{ nm}$) in powder and thin films on glass and Ag samples. The τ_{obs} obtained by fitting the sum of two exponential decays are included. The colors correspond to the different samples; red, orange: powder; cyan, blue: $22.5 \text{ molecules/nm}^2$ film on glass at RT, gray: $22.5 \text{ molecules/nm}^2$ film on Ag(111) at 4.5 K. The inset in f) shows an STM topography image of a $[\text{Eu(trensal)}]$ thin film on Ag(111) scanned at -10 V , 1 pA , indicating relatively stable conductivity.



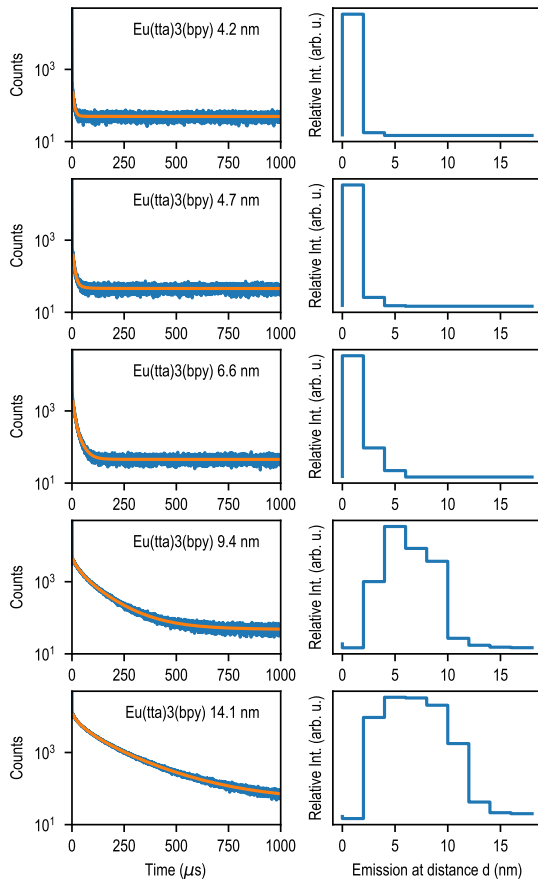


Figure 6: Experimental TCSPC data fitted with a sum of exponential decays (left panels) and corresponding thickness distribution extracted from the fit (right panels). The fit reveals the relative contribution from each layer.

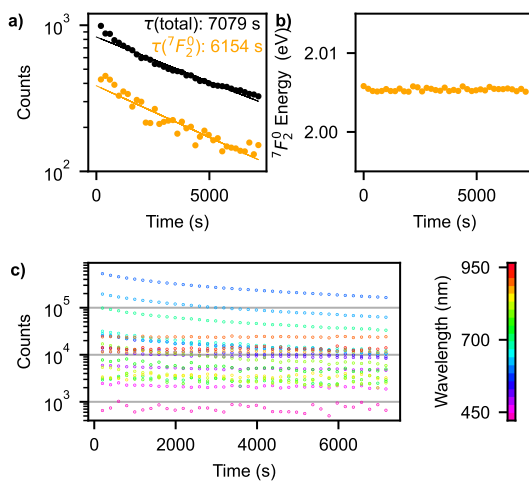


Figure 7: Decrease of photoluminescence intensity of a film of $[\text{Eu(tta)}_3(\text{bpy})]$ on $\text{Ag}(111)$ with a density of ~ 22.5 molecules/ $\text{nm}^2 \approx 21$ nm with time at 4.5 K under illumination (375 nm). a) Fluorescence intensity as a function of time integrated over all emission bands (black dots) and the most prominent $^5D_0 \rightarrow ^7F_2$ band (yellow dots). Exponential fits shown by solid lines. b) Peak position of the most prominent $^5D_0 \rightarrow ^7F_2$ band. c) Fluorescence intensity decreases at all wavelengths. The range from about 450 nm to about 950 nm has been divided into 20 equal bins.

Surface deposition and STM analysis

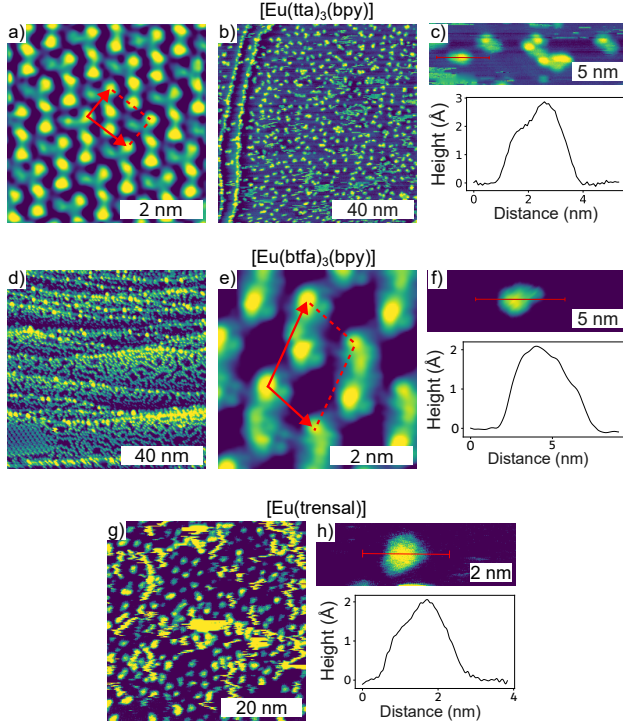


Figure 8: (a) Close-up STM image of lattice formation on a film of $[\text{Eu}(\text{tta})_3(\text{bpy})]$ on $\text{Ag}(111)$ sample with unit cell indicated in red. (2.0 V, 1 pA). (b) STM image of $[\text{Eu}(\text{tta})_3(\text{bpy})]$ on $\text{Au}(111)$ sublimed at 185 °C. (2.0 V, 10 pA). (c) Height profile across island of $[\text{Eu}(\text{tta})_3(\text{bpy})]$ on $\text{Ag}(111)$ sublimed at 185 °C after degassing the crucible at 150 °C for ~ 10 h. (2.0 V, 10 pA). (d) Large scale STM overview of $[\text{Eu}(\text{btfa})_3(\text{bpy})]$ close to 1 ML of on $\text{Ag}(111)$. (2.0 V, 10 pA) (e) Close-up STM image of lattice formation on a $[\text{Eu}(\text{btfa})_3(\text{bpy})]$ on $\text{Ag}(111)$ sample with unit cell indicated in red. (2.0 V, 10 pA). (f) Height profile across island of $[\text{Eu}(\text{btfa})_3(\text{bpy})]$ (2.0 V, 1 pA). (g) Large scale STM overview of $[\text{Eu}(\text{trensal})]$ on $\text{Au}(111)$. (2.0 V, 1 pA). (h) Height profile across a molecule on a $[\text{Eu}(\text{trensal})]$ on $\text{Au}(111)$ sample with corresponding STM image. (2.0 V, 1 pA).

The adsorption configuration of deposited molecular complexes is relevant for several reasons. As discussed above, the PL spectra shown in Fig. 3 and the corresponding decay experiments suggest a reduced symmetry in the sublimed films in comparison to powder, in case of films of $[\text{Eu}(\text{tta})_3(\text{bpy})]$ and $[\text{Eu}(\text{btfa})_3(\text{bpy})]$, but not in case of $[\text{Eu}(\text{trensal})]$. In addition, the orientation of the transition dipole moments influences the coupling of light to the underlying metal substrate and into the detection system. Therefore, it is worth investigating the adsorption and possible self-assembly of the molecules on the substrate with STM topography. We previously reported on the self assembly of Eu complexes,²⁷ including $[\text{Eu}(\text{tta})_3(\text{bpy})]$ and $[\text{Eu}(\text{btfa})_3(\text{bpy})]$. Recent

sublimation experiments at elevated temperatures (185 °C instead of 150 °C, degassing at 150 °C instead of 100 °C) revealed that sublimation of [Eu(tta)₃(bpy)] can result in the same pattern with the same unit cell (see Fig. 8 (b)) as those previously identified with [Eu(btfa)₃(bpy)].²⁷ In addition, at a sublimation temperature of 185 °C, the deposition of [Eu(tta)₃(bpy)] leads to a higher number of significantly larger objects without any apparent preferred orientation (see Fig. 8 (e,f)) which are likely to be entire complexes. This leads us to revise our previous conclusion and we now suggest that the self-assembled layers shown in b) and²⁷ are composed of fragments of the [Eu(tta)₃(bpy)] and [Eu(btfa)₃(bpy)] complexes. Bi-pyridine is part of both complexes and the observed pattern is in good agreement with 2,2,-bipyridine on Au(111).^{62,63}

Similarly, sublimation of [Eu(btfa)₃(bpy)] at 185 °C for 1 min shows a different structure formation than previously reported. The surface in some areas is covered with a lattice likely consisting of intact [Eu(btfa)₃(bpy)] complexes (Fig. 8 (g),(h)). The unit cell size is 3.73 nm² with two molecules per unit cell which is about three times larger than what we previously reported.²⁷

Sublimation of [Eu(trensal)] at a crucible temperature of 270 °C for ~ 9 s onto Au(111) at RT, resulted in a single type of homogeneously distributed molecules of approximately 2 Å height (Fig. 8 (i),(j)) without apparent preferred orientation. All three complexes show significant mobility in the STM junction, despite low temperature and low tunneling currents during scanning. Suitable complexes for single-molecule experiments would require increased stability both during the sublimation process and in terms of anchoring to the surface.

Conclusion

We have characterized the optical properties of sublimated thin films of three Eu³⁺ complexes on glass and Ag substrates and of varying thickness. In sublimated films, reduced order leads to broadening of individual bands and increased decay rates compared to microcrystallites in powder. In particular, coupling to the Ag(111) single crystal increases the total decay rate up to three orders of magnitude to about 1 MHz, although we do not yet see indications for exciton quenching via charge transport. An envisioned molecular complex in close contact to two metallic leads

is expected to decay at higher rates due to increased coupling, and molecular properties would need to be optimized accordingly. Quenching pathways in the kHz range such as coupling to vibrational modes, that determine the observed decay in powder or in solution, will be negligible, while molecular stability in direct vicinity of a metal and drastically reduced bleaching probability become essential. The observed efficient coupling to a metallic substrate is necessary to enhance the intrinsically low radiative rate of Eu³⁺ emitters and paves the way to effective single-molecule junctions optimized for efficient outcoupling of the plasmonic excitations to the far field.

Conflicts of interest

There are no conflicts to declare.

Acknowledgments

We acknowledge funding by the Deutsche Forschungsgemeinschaft (DFG, German Research Foundation) through the Collaborative Research Center “4 f for Future” (CRC 1573, project number 471424360) project C1 and C2 and support by the Helmholtz Association via the programs Natural, Artificial, and Cognitive Information Processing (NACIP) and Materials Systems Engineering (MSE).

References

- (1) Kuppusamy, S. K.; Hunger, D.; Ruben, M.; Goldner, P.; Serrano, D. Spin-bearing molecules as optically addressable platforms for quantum technologies. *Nanophotonics* **2024**, *13*, 4357–4379.
- (2) Song, N.; Wang, C.; Tang, Y. Smart Luminescent Materials Based on Rare-Earth Complexes:

From Precise Syntheses to Regulable Functions. *ACS Applied Materials & Interfaces* **2025**, *17*, 65386–65398.

- (3) Drexhage, K. Influence of a dielectric interface on fluorescence decay time. *Journal of Luminescence* **1970**, *1-2*, 693–701.
- (4) Noginova, N.; Barnakov, Y.; Li, H.; Noginov, M. A. Effect of metallic surface on electric dipole and magnetic dipole emission transitions in Eu³⁺ doped polymeric film. *Optics Express* **2009**, *17*, 10767–10772.
- (5) Worthing, P.; Amos, R.; Barnes, W. Modification of the spontaneous emission rate of Eu³⁺ ions embedded within a dielectric layer above a silver mirror. *Physical Review A* **1999**, *59*, 865–872.
- (6) Noginova, N.; Hussain, R.; Noginov, M. A.; Vella, J.; Urbas, A. Modification of electric and magnetic dipole emission in anisotropic plasmonic systems. *Metamaterials: Fundamentals and Applications V*. 2012; pp 85–90.
- (7) Chance, R. R.; Prock, A.; Silbey, R. *Advances in Chemical Physics*; John Wiley & Sons, Ltd, 1978; pp 1–65.
- (8) Kuhn, H. Classical Aspects of Energy Transfer in Molecular Systems. *The Journal of Chemical Physics* **1970**, *53*, 101–108.
- (9) MORAWITZ, H. Self-Coupling of a Two-Level System by a Mirror. *Phys. Rev.* **1969**, *187*, 1792–1796.
- (10) Amos, R. M.; Barnes, W. L. Modification of the spontaneous emission rate of Eu³⁺ ions close to a thin metal mirror. *Physical Review B* **1997**, *55*, 7249–7254, Publisher: American Physical Society.
- (11) Pockrand, I.; Brillante, A.; Möbius, D. Nonradiative decay of excited molecules near a metal surface. *Chemical Physics Letters* **1980**, *69*, 499–504.

(12) Ford, G. W.; Weber, W. H. Electromagnetic interactions of molecules with metal surfaces. *Physics Reports* **1984**, *113*, 195–287.

(13) Mor, D. C.; Aktug, G.; Schmidt, K.; Asokan, P.; Asai, N.; Huang, C.-J.; Dostalek, J. Plasmon-enhanced fluorescence (bio)sensors and other bioanalytical technologies. *TrAC Trends in Analytical Chemistry* **2025**, *183*, 118060.

(14) Ullah Khan, N.; Muhammad, Z.; Liu, X.; Lin, J.; Zheng, Q.; Zhang, H.; Malik, S.; He, H.; Shen, L. Ultrasensitive Detection of Exosome Using Biofunctionalized Gold Nanorods on a Silver-Island Film. *Nano Letters* **2021**, *21*, 5532 – 5539, Cited by: 25.

(15) Liang, L.; Lan, F.; Yin, X.; Ge, S.; Yu, J.; Yan, M. Metal-enhanced fluorescence/visual bi-modal platform for multiplexed ultrasensitive detection of microRNA with reusable paper analytical devices. *Biosensors and Bioelectronics* **2017**, *95*, 181–188.

(16) Pang, Y.; Rong, Z.; Wang, J.; Xiao, R.; Wang, S. A fluorescent aptasensor for H5N1 influenza virus detection based-on the core-shell nanoparticles metal-enhanced fluorescence (MEF). *Biosensors and Bioelectronics* **2015**, *66*, 527 – 532, Cited by: 172.

(17) Schmidt, K.; Riedel, T.; de los Santos Pereira, A.; Lynn, N. S.; Dorado Daza, D. F.; Dostalek, J. Sandwich Immuno-RCA Assay with Single Molecule Counting Readout: The Importance of Biointerface Design. *ACS Applied Materials and Interfaces* **2024**, *16*, 17109 – 17119, Cited by: 3; All Open Access, Green Open Access, Hybrid Gold Open Access.

(18) Kalinowski, J.; Stapor, W.; Cocchi, M.; Virgili, D.; Fattori, V. Electric-field-induced quenching of photoluminescence in photoconductive organic thin film structures based on Eu³⁺ complexes. *Journal of Applied Physics* **2006**, *100*, 034318.

(19) Campion, A.; Gallo, A.; Harris, C.; Robota, H.; Whitmore, P. Electronic energy transfer to metal surfaces: a test of classical image dipole theory at short distances. *Chemical Physics Letters* **1980**, *73*, 447–450.

(20) Kuhnke, K.; Becker, R.; Epple, M.; Kern, K. C 60 Exciton Quenching near Metal Surfaces. *Physical Review Letters* **1997**, *79*, 3246–3249.

(21) Knaak, T.; González, C.; Dappe, Y. J.; Harzmann, G. D.; Brandl, T.; Mayor, M.; Berndt, R.; Gruber, M. Fragmentation and Distortion of Terpyridine-Based Spin-Crossover Complexes on Au(111). *The Journal of Physical Chemistry C* **2019**, *123*, 4178–4185.

(22) Melo, L. L. L. S.; Castro, G. P. J.; Navarro, M.; Goncalves, S. M. C.; Simas, A. M. Unmasking the UV Photobleaching of β -Diketonate [Eu(BTFA)4]- Complexes as an Energy-Driven Photoreduction Process. *Inorganic Chemistry* **2025**, *64*, 3842–3856, Publisher: American Chemical Society.

(23) Chitnis, D.; Thejo Kalyani, N.; Dhoble, S. Comprehensive study on photophysical properties of Eu(TTA)3bipy phosphor molecularly doped in PMMA and PS matrices. *Results in Physics* **2019**, *13*, 102302.

(24) Chitnis, D.; Thejokalyani, N.; Dhoble, S. Exploration of spectroscopic properties of solvated tris(thenoyltrifluoroacetone)(2,2'-bipyridine)europium(III)red hybrid organic complex for solution processed OLEDs and displays. *Journal of Luminescence* **2017**, *185*, 61–71.

(25) Gameiro, C. G.; Achete, C. A.; Simão, R. A.; da Silva, E. F.; Santa-Cruz, P. A. Molecular UV dosimeters of lanthanide complex thin films: AFM as a function of ultraviolet exposure. *Journal of Alloys and Compounds* **2002**, *344*, 385–388, Proceedings of the Rare Earths' 2001 Conference.

(26) Liu, J.; Wang, K.; Zheng, W.; Huang, W.; Li, C.-H.; You, X.-Z. Improving spectral response of monocrystalline silicon photovoltaic modules using high efficient luminescent down-shifting Eu³⁺ complexes. *Progress in Photovoltaics: Research and Applications* **2013**, *21*, 668–675.

(27) Ebert, A.; Gerhard, L.; Feye, J.; Kuppusamy, S. K.; Brachnakova, B.; Ruben, M.;

Roesky, P. W.; Wulfhekel, W. Photoluminescence and self-assembly of three different Eu complexes. *Phys. Chem. Chem. Phys.* **2025**, *27*, 13984–13990.

(28) Batista, H. J.; de Andrade, A. V. M.; Longo, R. L.; Simas, A. M.; de Sá, G. F.; Ito, N. K.; Thompson, L. C. Synthesis, X-ray Structure, Spectroscopic Characterization, and Theoretical Prediction of the Structure and Electronic Spectrum of Eu(btfa)3bipy and an Assessment of the Effect of Fluorine as a β -Diketone Substituent on the Ligand-Metal Energy Transfer Process. *Inorganic Chemistry* **1998**, *37*, 3542–3547.

(29) de Sá, G. F.; Alves Jr, S.; da Silva, B. J.; da Silva Jr, E. F. A novel fluorinated Eu(III) β -diketone complex as thin film for optical device applications. *Optical Materials* **1998**, *11*, 23–28.

(30) Quirino, W.; Reyes, R.; Legnani, C.; Nóbrega, P.; Santa-Cruz, P.; Cremona, M. Eu- β -diketonate complex OLED as UV portable dosimeter. *Synthetic Metals* **2011**, *161*, 964–968.

(31) Kuppusamy, S. K.; Vasilenko, E.; Li, W.; Hessenauer, J.; Ioannou, C.; Fuhr, O.; Hunger, D.; Ruben, M. Observation of Narrow Optical Homogeneous Linewidth and Long Nuclear Spin Lifetimes in a Prototypical [Eu(trensal)] Complex. *The Journal of Physical Chemistry C* **2023**, *127*, 10670–10679, Publisher: American Chemical Society.

(32) Stoll, P.; Bernien, M.; Rolf, D.; Nickel, F.; Xu, Q.; Hartmann, C.; Umbach, T. R.; Kopprasch, J.; Ladenthin, J. N.; Schierle, E.; Weschke, E.; Czekelius, C.; Kuch, W.; Franke, K. J. Magnetic anisotropy in surface-supported single-ion lanthanide complexes. *Physical Review B* **2016**, *94*, 224426.

(33) Edelmann, K.; Gerhard, L.; Winkler, M.; Wilmes, L.; Rai, V.; Schumann, M.; Kern, C.; Meyer, M.; Wegener, M.; Wulfhekel, W. Light collection from a low-temperature scanning tunneling microscope using integrated mirror tips fabricated by direct laser writing. *Review of Scientific Instruments* **2018**, *89*, 123107, Publisher: American Institute of Physics.

(34) Chitnis, D.; Kalyani, N. T.; Dhoble, S. Portrayal of structural, thermal and optical properties of pH sensitive Eu(TTA)3bipy hybrid organic complex for OLEDs. *Optik* **2017**, *130*, 237–244.

(35) Seward, C.; Wang, S. Dimeric and polymeric [Eu(tta)₃ L] complexes (tta = thenoyltrifluoroacetone, L = 4,4' -bipyridine, *trans* -1,2-bis(4-pyridyl)ethylene, 4,4' -bipyridine- *N*, *N*' -dioxide). *Canadian Journal of Chemistry* **2001**, *79*, 1187–1193.

(36) Binnemans, K. Interpretation of europium(III) spectra. *Coordination Chemistry Reviews* **2015**, *295*, 1–45.

(37) Horrocks, W. D.; Sudnick, D. R. Lanthanide ion probes of structure in biology. Laser-induced luminescence decay constants provide a direct measure of the number of metal-coordinated water molecules. *Journal of the American Chemical Society* **1979**, *101*, 334–340.

(38) Kunz, R. E.; Lukosz, W. Changes in fluorescence lifetimes induced by variable optical environments. *Physical Review B* **1980**, *21*, 4814–4828.

(39) Porcher, P.; Caro, P. Influence of J-mixing on the phenomenological interpretation of the Eu³⁺ ion spectroscopic properties. *Journal of Luminescence* **1980**, *21*, 207 – 216, Cited by: 101.

(40) Tanaka, M.; Nishimura, G.; Kushida, T. Contribution of J mixing to the 5D0-7F0 transition of Eu³⁺ ions in several host matrices. *Physical Review B* **1994**, *49*, 16917 – 16925, Cited by: 136.

(41) Tanaka, M.; Kushida, T. Effects of static crystal field on the homogeneous width of the 5D0-7F0 line of Eu³⁺ and Sm²⁺ in solids. *Physical Review B* **1995**, *52*, 4171 – 4178, Cited by: 23.

(42) Malta, O. Lanthanide f-f transitions hypersensitive to the environment. *Molecular Physics* **1981**, *42*, 65 – 72, Cited by: 49.

(43) Chen, X.; Liu, G. The standard and anomalous crystal-field spectra of Eu³⁺. *Journal of Solid State Chemistry* **2005**, *178*, 419–428, f-element Spectroscopy and Coordination Chemistry.

(44) Borges, A. S.; Caliman, E. V.; Dutra, J. D. L.; Da Silva, J. G.; Araujo, M. H. Structure and luminescent investigation of new Ln(III)-TTA complexes containing N-methyl- ϵ -caprolactam as ligand. *Journal of Luminescence* **2016**, *170*, 654–662, SI: Lanthanide spectroscopy.

(45) Görller-Walrand, C.; Fluyt, L.; Ceulemans, A.; Carnall, W. Magnetic dipole transitions as standards for Judd-Ofelt parametrization in lanthanide spectra. *The Journal of Chemical Physics* **1991**, *95*, 3099 – 3106, Cited by: 157.

(46) Philpott, M. R. Fluorescence from molecules between mirrors. *Chemical Physics Letters* **1973**, *19*, 435–439.

(47) Hussain, R.; Keene, D.; Noginova, N.; Durach, M. Spontaneous emission of electric and magnetic dipoles in the vicinity of thin and thick metal. *Optics Express* **2014**, *22*, 7744–7755.

(48) Novotny, L.; Hecht, B. *Principles of Nano-Optics*, 2nd ed.; Cambridge University Press: Cambridge, 2012.

(49) Lakowicz, J. R.; Shen, Y.; D'Auria, S.; Malicka, J.; Fang, J.; Gryczynski, Z.; Gryczynski, I. Radiative Decay Engineering: 2. Effects of Silver Island Films on Fluorescence Intensity, Lifetimes, and Resonance Energy Transfer. *Analytical Biochemistry* **2002**, *301*, 261–277.

(50) Chigrin, D. N.; Kumar, D.; Cuma, D.; von Plessen, G. Emission Quenching of Magnetic Dipole Transitions near a Metal Nanoparticle. *ACS Photonics* **2016**, *3*, 27–34.

(51) Bharadwaj, P.; Novotny, L. Spectral dependence of single molecule fluorescence enhancement. *Optics Express* **2007**, *15*, 14266–14274, Publisher: Optica Publishing Group.

(52) Faggiani, R.; Yang, J.; Lalanne, P. Quenching, Plasmonic, and Radiative Decays in Nanogap Emitting Devices. *ACS Photonics* **2015**, *2*, 1739–1744, Publisher: American Chemical Society.

(53) Campion, A.; Gallo, A.; Harris, C.; Robota, H.; Whitmore, P. Electronic energy transfer to metal surfaces: a test of classical image dipole theory at short distances. *Chemical Physics Letters* **1980**, *73*, 447–450.

(54) Yang, H. U.; D'Archangel, J.; Sundheimer, M. L.; Tucker, E.; Boreman, G. D.; Raschke, M. B. Optical dielectric function of silver. *Physical Review B* **2015**, *91*, 235137.

(55) Nockemann, P.; Beurer, E.; Driesen, K.; Van Deun, R.; Van Hecke, K.; Van Meervelt, L.; Binnemans, K. Photostability of a highly luminescent europium β -diketonate complex in imidazolium ionic liquids. *Chem. Commun.* **2005**, 4354–4356.

(56) Jiménez, G. L.; Reyes-Rodríguez, J.; Padilla, I.; Alarcón-Flores, G.; Falcony, C. Reducing the photo-bleaching effect of a new europium complex embedded in styrene butadiene copolymer. *Optical Materials* **2018**, *76*, 271–277.

(57) Pagnot, T.; Audebert, P.; Tribillon, G. Photostability study of europium dibenzolymethide embedded in polystyrene thin films with high concentration. *Chemical Physics Letters* **2000**, *322*, 572–578.

(58) Gameiro, C.; da Silva, E.; Alves, S.; de Sá, G.; Santa-Cruz, P. Lanthanide complexes dispersed in enamel: a promising new material for photonic devices. *Journal of Alloys and Compounds* **2001**, *323-324*, 820–823, Proceedings of the 4th International Conference on f-Elements.

(59) Xu, Q.; Li, L.; Li, B.; Yu, J.; Xu, R. Encapsulation and luminescent property of tetrakis (1-(2-thenoyl)-3,3,3-trifluoracetate) europium N-hexadecyl pyridinium in modified Si-MCM-41. *Microporous and Mesoporous Materials* **2000**, *38*, 351–358.

(60) Lima, P. P.; Nolasco, M. M.; Paz, F. A. A.; Ferreira, R. A. S.; Longo, R. L.; Malta, O. L.; Carlos, L. D. Photo-Click Chemistry to Design Highly Efficient Lanthanide β -Diketonate Complexes Stable under UV Irradiation. *Chemistry of Materials* **2013**, *25*, 586–598.

(61) Eggeling, C.; Widengren, J.; Rigler, R.; Seidel, C. A. M. Photobleaching of Fluorescent Dyes under Conditions Used for Single-Molecule Detection: Evidence of Two-Step Photolysis. *Analytical Chemistry* **1998**, *70*, 2651–2659, Publisher: American Chemical Society.

(62) Dretschkow, T.; Lampner, D.; Wandlowski, T. Structural transitions in 2,2'-bipyridine adlayers on Au(111)—an in-situ STM study¹This paper is dedicated to MJE, who contributed to the manuscript in a special way.¹ *Journal of Electroanalytical Chemistry* **1998**, *458*, 121–138.

(63) Cunha, F.; Tao, N. J.; Wang, X. W.; Jin, Q.; Duong, B.; D'Agnese, J. Potential-Induced Phase Transitions in 2,2'-Bipyridine and 4,4'-Bipyridine Monolayers on Au(111) Studied by in Situ Scanning Tunneling Microscopy and Atomic Force Microscopy. *Langmuir* **1996**, *12*, 6410–6418.